Monthly Notices
of the
ROYAL ASTRONOMICAL SOCIETY

MNRAS **482,** 4146–4154 (2019)
Advance Access publication 2018 October 29

doi:10.1093/mnras/sty2830

Hidden planetary friends: on the stability of two-planet systems in the presence of a distant, inclined companion

Paul Denham,[1]★ Smadar Naoz,[1,2]★ Bao-Minh Hoang,[1] Alexander P. Stephan[1] and Will M. Farr[3]

[1]*Physics and Astronomy Department, University of California, Los Angeles, CA 90024, USA*
[2]*Department of Physics and Astronomy, Mani L. Bhaumik Institute for Theoretical Physics, UCLA, Los Angeles, CA 90095, USA*
[3]*School of Physics and Astronomy, University of Birmingham, Birmingham B15 2TT, UK*

Accepted 2018 October 8. Received 2018 October 8; in original form 2018 February 2

ABSTRACT

Recent observational campaigns have shown that multiplanet systems seem to be abundant in our Galaxy. Moreover, it seems that these systems might have distant companions, either planets, brown-dwarfs, or other stellar objects. These companions might be inclined with respect to the inner planets, and could potentially excite the eccentricities of the inner planets through the Eccentric Kozai–Lidov mechanism. These eccentricity excitations could perhaps cause the inner orbits to cross, disrupting the inner system. We study the stability of two-planet systems in the presence of a distant, inclined, giant planet. Specifically, we derive a stability criterion, which depends on the companion's separation and eccentricity. We show that our analytic criterion agrees with the results obtained from numerically integrating an ensemble of systems both secularly and with *N*-body simulations. Finally, as a potential proof-of-concept, we provide a set of predictions for the parameter space that allows the existence of planetary companions for the Kepler-56, Kepler-448, Kepler-88, Kepler-109, and Kepler-36 systems.

Key words: planets and satellites: dynamical evolution and stability – planet–star interactions – stars: kinematics and dynamics – planetary systems.

1 INTRODUCTION

Recent ground- and space-based observations have shown that multiplanet systems are abundant around main-sequence stars (e.g. Howard et al. 2010, 2012; Borucki et al. 2011; Lissauer et al. 2011; Mayor et al. 2011; Youdin 2011; Batalha et al. 2013; Dressing & Charbonneau 2013; Petigura, Howard & Marcy 2013; Christiansen et al. 2015). These studies reveal that the architecture of planetary systems can drastically vary from our Solar system. For example, systems consisting of multiple low-mass (sub-Jovian) planets with relatively compact orbits usually have periods that are shorter than Mercury's.

NASA's Kepler mission found an abundance of compact multiplanet super-Earths or sub-Neptune systems (e.g. Mullally et al. 2015; Burke et al. 2015; Morton et al. 2016; Hansen 2017). These systems seemed to have low eccentricities (e.g. Lithwick, Xie & Wu 2012; Van Eylen & Albrecht 2015). In addition, it was suggested that these many body systems are close to the dynamically stable limit (e.g. Fang & Margot 2013; Pu & Wu 2015; Volk & Gladman 2015). It was also proposed that single planet systems might be the product of systems initially consisting of multiple planets that underwent a period of disruption, i.e. collisions, resulting in reducing the number of planets (see Johansen et al. 2012; Becker & Adams 2016).

Giant planets may play a key role in forming inner planetary systems. Radial velocity surveys, along with the existence of Jupiter, have shown giants usually reside at larger distances from their host star than other planets in the system ($\geq$1 au) (e.g. Knutson et al. 2014; Bryan et al. 2016). For example, there were some suggestions that the near-resonant gravitational interactions between giant outer planets and smaller inner planets can shape the configuration of an inner system's asteroid belt (e.g. Williams & Faulkner 1981; Minton & Malhotra 2011). Hence, it was suggested that our Solar system's inner planets are of a second generation, which came after Jupiter migrated inwards to its current orbit (e.g. Batygin & Laughlin 2015). Furthermore, secular resonance may be the cause of water being delivered to Earth (Scholl & Froeschle 1986; Morbidelli 1994), the potential instability of Mercury's orbit (Neron de Surgy & Laskar 1997; Fienga et al. 2009; Batygin & Laughlin 2008; Lithwick & Wu 2011), and the obliquity of the exoplanets in general (e.g. Naoz et al. 2011; Li et al. 2014b).

Recently, several studies showed that the presence of a giant planet can affect the ability to detect an inner system (e.g. Becker & Adams 2017; Hansen 2017; Huang, Petrovich & Deibert 2017; Jontof-Hutter et al. 2017; Mustill, Davies & Johansen 2017).

★ E-mail: Pdenham629@gmail.com (PD); snaoz@astro.ucla.edu (SN)

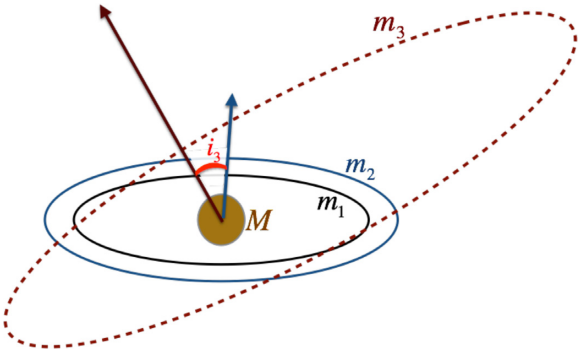

Figure 1. Here is a schematic of the systems being analysed. The inclination of the third planet, i_3, is shown and measured relative to the z-axis, along the spin axis of the host star. M, m_1, m_2, and m_3 are the masses of the host star, and the first, second, and third planets, respectively.

Specifically, dynamical interactions from a giant planet, having a semimajor axis much greater than the planets in the inner system, can excite eccentricities and inclinations of the inner planets. A possible effect is that the inner system becomes incapable of having multiple transits or completely unstable. Volk & Gladman (2015) showed that observed multiplanet systems may actually be the remnants of a compact system that was tighter in the past but lost planets through dynamical instabilities and collisions (see also Petrovich, Tremaine & Rafikov 2014). Interestingly, verifying these problems could reconcile the Kepler dichotomy (e.g. Johansen et al. 2012; Ballard & Johnson 2016; Hansen 2017) and may also explain some of the diverse bulk compositions observed in multiple planet systems (e.g. Inamdar & Schlichting 2016).

In this work, we investigate the stability of compact sub-Jovian inner planetary systems in the presence of a distant giant planet (see Fig. 1 for an illustration of the system). Over long time-scales, a distant giant planet's gravitational perturbations can excite the eccentricities of the inner planet's to high values, destabilizing the inner system (e.g. Naoz et al. 2011). However, if the frequency of angular momentum exchange between the inner planets is sufficiently high, then the inner system can stabilize. Below we derive an analytic stability criterion (Section 2). Then we analyse our nominal system in Section 3 and provide specific predictions for Kepler systems in Section 3.3. Finally, we offer our conclusion in Section 4.

Near the completion of this work, we became aware of a complementary study of stability in similar systems (Pu & Lai 2018). Here, we provide a comprehensive stability criterion as a function of the companion's parameters. Furthermore, we provide a set of predictions for possible hidden companion orbits in several observed systems.

2 ANALYTICAL STABILITY CRITERION

Here, we develop a generic treatment of the stability of two-body systems in the presence of an inclined outer planet. Consider an inner system consisting of two planets (m_1 and m_2) orbiting around a host star M with a relatively tight configuration (with semimajor axis a_1 and a_2, respectively). We introduce an inclined and eccentric companion that is much farther from the host star than the planets in the inner system (m_3 and a_3, see Fig. 1 for an illustration of the system). We initialize this system to have orbits far from mean-motion resonance, and have $a_1, a_2 \ll a_3$. The three planets' orbits have corresponding eccentricities e_1, e_2, and e_3. We set an arbitrary z-axis to be perpendicular to the initial orbital plane of the inner two planets, thus, the inclinations of m_1, m_2, and m_3 are defined as i_1, i_2 and i_3. Accordingly, for planets one, two, and three we denote the longitude of ascending nodes and the argument of periapse Ω_1, Ω_2, Ω_3, ω_1, ω_2, and ω_3.

The outer orbit can excite the eccentricities, via the EKL (Kozai 1962, Lidov 1962, see Naoz 2016 for review) on each planet in the inner system. The EKL resonance causes angular momentum exchange between the outer and inner planets, which in turn causes precession of the periapse of each of the inner orbits. However, angular momentum exchange between the inner two planets also induces precession of the periapse (the so-called Laplace–Lagrange interactions, e.g. Murray & Dermott 2000). If the inner orbits' angular momentum exchange takes place at a faster rate than that induced by the outer companion, then the system will not be disrupted by perturbations from the tertiary planet. The quadrupole approximation to the time-scale of the EKL between the third planet m_3 and the second one, m_2 is given by

$$\tau_{k(2,3)} \sim \frac{16}{15}\frac{a_3^3}{a_2^{3/2}}\frac{\sqrt{M+m_2+m_1}}{m_3\sqrt{G}}\left(1-e_3^2\right)^{3/2} \tag{1}$$

(e.g. Antognini 2015) where G is the gravitational constant. This is roughly the time-scale at which the second planet's argument of periapse precesses. Note that here we considered the time-scale of EKL excitations from the tertiary on m_2 since this time-scale is shorter than the time-scale of EKL excitations between m_3 and m_1. Planet m_2's argument of periapse also precesses due to gravitational perturbations from the innermost planet, m_1. The associated time-scale is (e.g. Murray & Dermott 2000)

$$\tau_{LL} \sim \left[A_{22}+A_{21}\left(\frac{e_1}{e_2}\right)\cos(\varpi_2-\varpi_1) - B_{22}-B_{21}\left(\frac{i_1}{i_2}\right)\cos(\Omega_2-\Omega_1)\right]^{-1}, \tag{2}$$

where $\varpi_j = \omega_j + \Omega_j$ for $j = 1, 2$. The $A_{i,j}$ and $B_{i,j}$ are Laplace coefficients, which are determined by

$$A_{22} = n_2\frac{1}{4\pi}\frac{m_1}{M+m_2}\left(\frac{a_1}{a_2}\right)^2 f_\psi, \tag{3}$$

$$A_{21} = -n_2\frac{1}{4\pi}\frac{m_1}{M+m_2}\left(\frac{a_1}{a_2}\right) f_{2\psi}, \tag{4}$$

$$B_{22} = -n_2\frac{1}{4\pi}\frac{m_1}{M+m_2}\left(\frac{a_1}{a_2}\right)^2 f_\psi, \tag{5}$$

$$B_{21} = n_2\frac{1}{4\pi}\frac{m_1}{M+m_2}\left(\frac{a_1}{a_2}\right) f_\psi, \tag{6}$$

and

$$f_\psi = \int_0^{2\pi}\frac{\cos\psi}{\left(1-2\left(\frac{a_1}{a_2}\right)\cos\psi+\left(\frac{a_1}{a_2}\right)^2\right)^{\frac{3}{2}}}\mathrm{d}\psi, \tag{7}$$

$$f_{2\psi} = \int_0^{2\pi}\frac{\cos 2\psi}{\left(1-2\left(\frac{a_1}{a_2}\right)\cos\psi+\left(\frac{a_1}{a_2}\right)^2\right)^{\frac{3}{2}}}\mathrm{d}\psi. \tag{8}$$

The system will remain stable if angular momentum exchange between the two inner planets takes place faster than the precession induced by m_3. Accordingly, there exists two regions of parameter

space: one contains systems where perturbations on m_2 are dominantly from m_1 and the other contains systems where m_2 is dominated by m_3. The former is called the Laplace–Lagrange region, and the latter is called the EKL region. The transition between the Laplace–Lagrange region and EKL region is determined by comparing the two time-scales relating the frequencies of precession from each mechanism, i.e.

$$\tau_k \sim \tau_{\rm LL}. \tag{9}$$

We have related the time-scale for Kozai oscillations induced by m_3 on m_2 to the Laplace–Lagrange time-scale between m_1 and m_2. Equating these time-scales yields a simple expression for the critical eccentricity of the third planet, $e_{3,c}$, as a function of a_2, i.e.

$$e_{3,c} \sim \left(1 - \left[\frac{15}{16}\frac{m_3\sqrt{G}}{\sqrt{M+m_1+m_2}}\frac{a_2^{3/2}}{a_3^3}\frac{1}{f_{\rm LL}}\right]^{\frac{2}{3}}\right)^{\frac{1}{2}}, \tag{10}$$

where

$$f_{\rm LL} = A_{22} + A_{21}\frac{e_{1,\rm ic}}{e_{2,\rm ic}}\cos(\varpi_1-\varpi_2) - B_{21}\frac{i_{1,\rm ic}}{i_{2,\rm ic}}\cos(\Omega_1-\Omega_2) - B_{22}. \tag{11}$$

$e_{j,\rm ic}$ and $i_{j,\rm ic}$ are the initial eccentricity and inclination for the two inner planets, i.e. $j = 1, 2$. As we show below, during the evolution of a stable system $\Omega_1 \sim \Omega_2$, $\varpi_2 \sim \varpi_1$, $e_1 \sim e_2$, and $i_1 \sim i_2$. Thus, we define a minimum stable configuration of $f_{\rm LL,min}$

$$f_{\rm LL,min} = A_{22} + \frac{e_{1,\rm ic}}{e_{2,\rm ic}}A_{21} - \frac{i_{1,\rm ic}}{i_{2,\rm ic}}B_{21} - B_{22}. \tag{12}$$

Numerically we find that during the evolution of an unstable system, $e_1/e2$, i_1/i_2, Ω_1/Ω_2, and ϖ_2/ϖ_1 largely deviate from unity, where $\cos(\varpi_1 - \varpi_2)$ can be negative. Thus, we also define the maximum stability as

$$f_{\rm LL,max} = A_{22} - \frac{e_{1,\rm ic}}{e_{2,\rm ic}}A_{21} - \frac{i_{1,\rm ic}}{i_{2,\rm ic}}B_{21} - B_{22}, \tag{13}$$

where the difference between equations (12) and (13) is the sign of A_{21}. The stability of systems transitions from the minimum to the maximum $f_{\rm LL}$, as a function of e_3. In other words we find a band of parameter space, between $e_{3,c}(f_{\rm LL,min})$ and $e_{3,c}(f_{\rm LL,max})$, where systems are nearly unstable or completely unstable. If the third planet's eccentricity is larger than the right-hand side of equation (10), then the inner system is more likely to become unstable. In the next section, we test this stability criterion and show that it agrees with secular numerical integration.

We note that this stability criterion is based on the Laplace–Lagrange approximation, which assumes small eccentricities and inclinations for orbits in the inner system. Thus, it might break down for initial large eccentricities or mutual inclinations of the inner two planets. Furthermore, this stability criterion assumes that the inner system is compact and that the eccentricity excitations from the second planet on the first are suppressed. On the other hand, in the presence of these conditions the stability criterion depends only on the shortest EKL time-scale induced by the far away companion and the corresponding Laplace–Lagrange time-scale. Thus, it is straightforward to generalize it to more than two inner planets.

3 LONG-TERM STABILITY OF MULTIPLANET SYSTEM

3.1 The Gaussian averaging method

To test our analytic stability criterion we utilize Gauss's method. This prescription allows us to integrate the system over a long time-scale (set to be 10 Gyr, see below), in a time-efficient way. In this mathematical framework, the non-resonant planets' orbits are phase-averaged and are treated as massive, pliable wires interacting with each other. The line-density of each wire is inversely proportional to the orbital velocity of each planet. The secular, orbit-averaged method requires that the semimajor axes of the wires are constants of motion. We calculate the forces that different wires exert on each other over time.

This method was recently extended to include softened gravitational interactions by introducing a small parameter in the interaction potentials to avoid possible divergences while integrating (Touma, Tremaine & Kazandjian 2009). Furthermore, the method has been proven to be very powerful in addressing different problems in astrophysics, ranging from understanding the dynamics in galactic nuclei to describing how debris discs evolve (e.g. Touma et al. 2009; Nesvold et al. 2016; Sridhar & Touma 2016; Saillenfest et al. 2017).

3.2 Stability test on a nominal system

We tested our stability criterion by using the aforementioned Gaussian averaging method to numerically integrate an ensemble of systems with identical initial conditions except for the semimajor axis and eccentricity of the second and third planets, respectively. In this ensemble, we initialize all systems with a primary star $M = 1\,{\rm M}_\odot$ orbited by three planets where the two inner planets, m_1, and m_2, each have masses of $1\,{\rm M}_\oplus$. The innermost planet, m_1, was placed in an orbit with a semimajor axis of $a_1 = 1$ au, and both inner planets were set initially on *nearly circular orbits* ($e_1 = e_2 = 0.001$) in the same orbital plane. We set the third planet with a mass of $m_3 = 1\,{\rm M}_J$, at $a_3 = 100$ au. Throughout the ensemble, a_2 ranges from 1.4 to 5.9 au, in steps of 0.5 au, and e_3 ranges from 0 to 0.95 in steps of 0.05. In all such systems, the third planet's inclination was set to be 45° relative to the inner system. We integrated each system to 10 Gyr, or until orbits crossed. From the results we made a grid labelling the stable/unstable systems of the ensemble. The grid revealed that stable orbits are bounded by the stability criterion. The same process was done on an ensemble which had the third planet's inclination set to 65° instead; the result was the same.

We also check for consistency of our results with direct *N*-body calculation using the REBOUND software (e.g. Rein & Liu 2012). As mentioned, all of our secular runs were integrated up to 10 Gyr or until we achieved orbit crossing, however, this is a numerically expansive practice. Thus, using REBOUND we have numerically integrated the slice of the parameter space with a_2 fixed to 4.9 au. The integration carried on to either orbit crossing or up to 80 Myr. We note that $log(1-\delta)$ values from *N*-body calculations are in agreement with those found from the orbit averaging code (not shown in Fig. 2 to avoid clutter).

In Fig. 2, we show the grid of systems we integrated in the parameter space relating a_2 and e_3. The colour code is determined by a proxy that characterizes the stability of the system. The proxy is defined as $\log(1-\delta)$, where δ is a parameter which describes

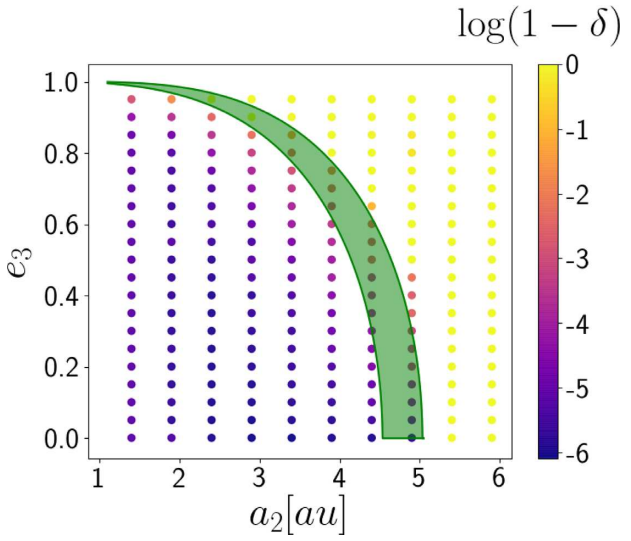

Figure 2. Here is the parameter space relating the third planet's eccentricity with the second planet's separation. The distant companion's inclination was set to 45°. The colour code shows $\log(1-\delta)$, equation (14). This parameter serves as a proxy for how close the two inner orbits came to each other during the evolution. A darker colour characterizes far away separation while a lighter colour characterizes orbit crossing. The stability criterion, equation (10), is plotted over the grid to show that stable orbits are bounded. The bottom green line represents $e_{3,c}(f_{LL,min})$ and the top green line represents $e_{3,c}(f_{LL,max})$, and thus the shaded band is the transition zone (see the text). Systems above the zone undergo an instability episode while systems below the zone are stable.

how close the two inner orbits came during the evolution:

$$\delta = \min\left[\frac{a_2(1-e_2)-a_1(1+e_1)}{a_2-a_1}\right]. \quad (14)$$

In Fig. 2, a lighter colour means a smaller value of δ, which when zero yields orbit crossing, while a darker colour represents a stable configuration. The criterion for stability is plotted over the grid to show that it is in agreement with the probability for orbits to cross. Above the stability curve, systems are more likely to destabilize during evolution.

The proxy also reveals a transitional zone of the parameter space. This zone agrees with our analytically determined zone [i.e. between $e_{3,c}(f_{LL,min})$ and $e_{3,c}(f_{LL,max})$], where, given the initial conditions in the numerical runs, we set $e_{1,ic}/e_{2,ic} \sim 1$ and $i_{1,ic}/i_{2,ic} \sim 1$. Closer to the stability curve, the orbits might get their eccentricities excited and periodically move closer to one another, but their orbits may never cross. Moreover, far into the top right of Fig. 2, the instability will take place sooner in the evolution. In this region, the two inner orbits will undergo Eccentric Kozai–Lidov (EKL) evolution independently of each other.

The third planet can excite the inner planet's eccentricities on the EKL time-scale. However, eccentricity excitations of each planet will not necessarily cause orbit crossing, as depicted in Fig. 2. In the parameter space for our ensemble, we have identified a region containing stable systems that seems to smoothly transition into the instability region. Hence, we identify three regimes: the stable regime, the intermediate regime, and the unstable regime. In the stable regime, the Laplace–Lagrange rapid angular momentum exchange between the two inner planets dominates over the gravitational perturbations of the outer orbit. The left column of Fig. 3 depicts this evolution; the system in this column resides in the bottom left of the parameter space in Fig. 2. The system remains stable for 10 Gyr of evolution and the orbits never come close to one another. The two inner planets' inclinations oscillate together around the initial z-axis, due to the precession of the nodes (see below). In the intermediate region, systems might appear to be stable for a long time but the outer orbit perturbations become too dominant, causing instability of the inner system. We show the dynamics of this type of evolution in the middle panel of Fig. 3. This system resides very close to the stability criterion plotted in Fig. 2, inside the transition zone between $e_{3,c}(f_{LL,min})$ and $e_{3,c}(f_{LL,max})$. In the unstable regime, gravitational perturbations from the third planet cause high amplitude eccentricity excitation in the inner planets, causing orbits to cross. We show this behaviour in the right column 3. This system lies in the top right of the parameter space depicted in Fig. 2.

In the system's reference frame (see Fig. 1), the inner planet's inclinations are the angles between their respective angular momenta and the normal to the *initial* orbits. Thus, the inclination modulation shown in the stable system (the left column in Fig. 3, is due to precession of the nodes, which results in maximum inclination, which is $\sim 2 \times i_3$, since we have started with $i_{3,0} = 45°$ (e.g. Innanen et al. 1997). In contrast, the unstable regime results in misalignment between the inner two planets.

3.3 Applications: predictions for observed systems

The stability criterion derived here can be used to predict the parameter space in which a hidden companion can exist within a system without destabilizing it. As a proof-of-concept, we discuss the stability of a few non-resonant observed exoplanetary systems in the presence of inclined planets. Specifically, for some observed systems, we provide a set of predictions that characterize the ranges of parameter space available for hidden companions to exist in without disrupting inner orbits. We focus on the following systems: Kepler-419, Kepler-56, Kepler-448, and Kepler-36. These represent the few systems that characterize the extreme limits of two-planet systems, from tightly packed super-Earths such as Kepler-36 to hierarchical eccentric warm Jupiter systems such as Kepler-448. In Fig. 4, we show the relevant parameter space in which the systems can have a hidden inclined companion and remain stable. We chose the more conservative stability criterion for this exercise, i.e. $e_{3,c}(f_{LL,min})$. Each line in the four panels of Fig. 4 shows the stability criterion for different companion masses. In particular, we consider companion masses of (from top to bottom), 0.1, 0.5, 1, 5, and 20 M_J. For each companion mass, allowed system configurations lie below the curve, and unstable configurations are above the curve. We caution that very close to the stability curve (even below the curve) systems may still undergo eccentricity excitations that may affect the dynamics. The parameters of the inner, observed planets were taken from observations, see Table 1. Below we discuss the specifics of the four example systems.

(i) *Kepler-36* is an, approximately, one solar mass star orbited by two few-Earth mass planets on 13.8 and 16.2 d orbits (Carter et al. 2012). This compact configuration is expected to be stable in the presence of perturbations as shown in Fig. 4, in the top left panel. For example, as can be seen in the figure, an eccentric inclined 20 M_J brown dwarf can reside slightly beyond 2 au.

(ii) *Kepler-56* is an evolved star ($M = 1.37\ M_\odot$) at the base of the red giant branch and is orbited by two sub-Jovian planets with low mutual inclinations (e.g. Huber et al. 2013). Most notably, asteroseismology analysis placed a lower limit on the two planets' obliquities of 37°. Li et al. (2014b) showed that a large obliquity

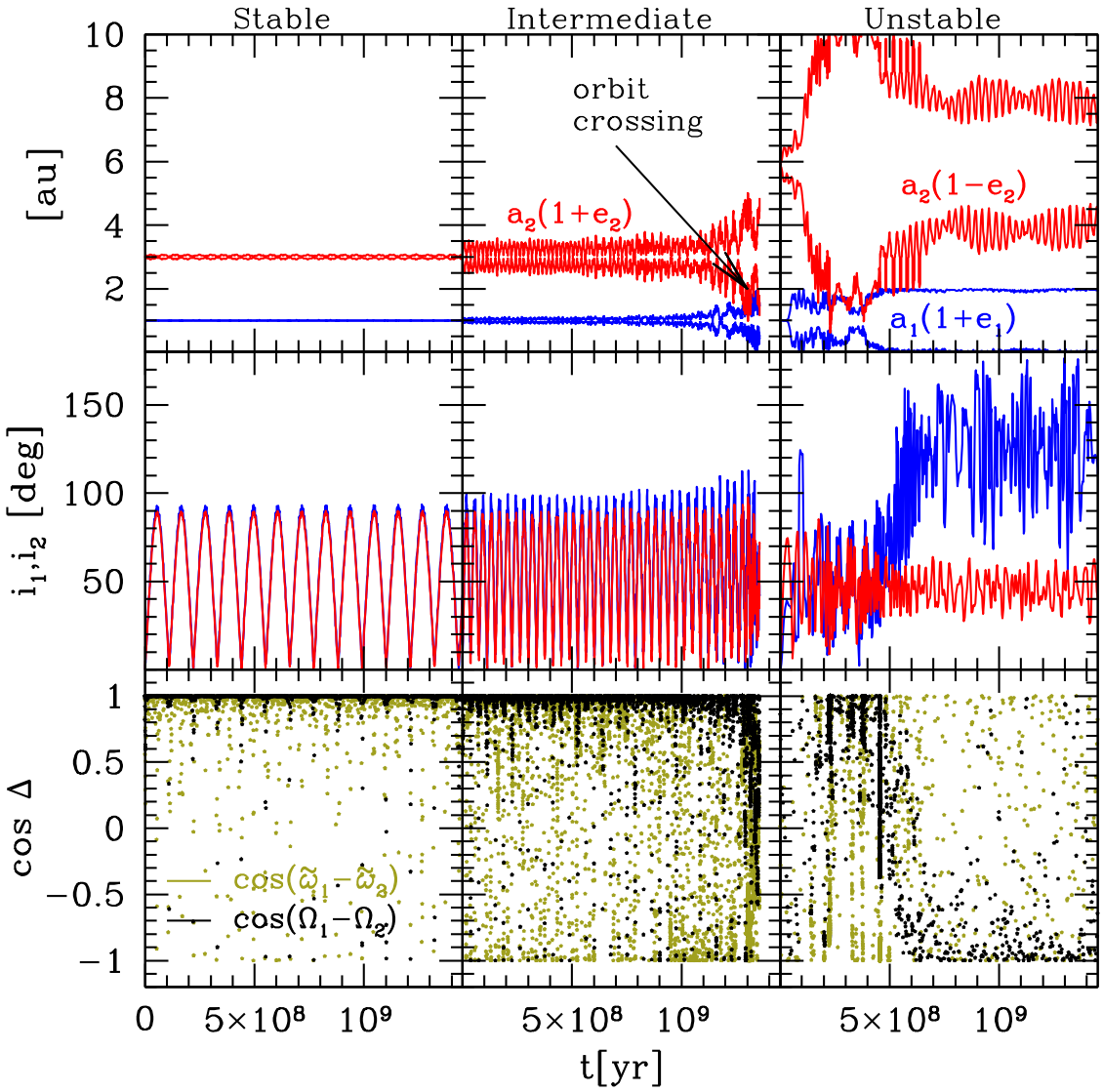

Figure 3. Here are the three prominent types of dynamics from each region. From left to right, stable, intermediate, and unstable, for our nominal system. Shown in the top panels are the apocentres and the pericentres of the innermost planets (m_1 in blue and m_2 in red). The middle panels show the inclinations of the inner planets (i_1 in blue and i_2 in red). *Note that this inclination is not with respect to the total angular momentum, but rather with respect to the initial angular momentum of the two inner planets.* The bottom panels show, coloured in black, the difference between the longitude of ascending nodes of the two inner planets as $\cos(\Omega_1 - \Omega_2)$, and, in yellow, the difference between the longitude of the periapsis as $\cos(\varpi_1 - \varpi_2)$. These two parameters are present in equation (11). Recall that the nominal system has the following parameters: $M = 1\ \mathrm{M}_\odot$, $m_1 = m_2 = 1\ \mathrm{M}_\oplus$, $m_3 = 1\ \mathrm{M}_J$, $a_1 = 1$ au, $a_3 = 100$ au, and we set initially $\omega_1 = \omega_2 = \omega_3 = \Omega_1 = \Omega_2 = \Omega_3 = 0$, $e_1 = e_2 = 0.001$, $i_1 = i_2 = 0.001$ and $i_3 = 45^\circ$. The only difference between each integrated system is the second planet's separation and the third planet's eccentricity. For the *stable* system we chose $a_2 = 3$ au and $e_3 = 0.8$. For the *intermediate* system we had $a_2 = 3$ au and $e_3 = 0.9$ (which placed it on the stability curve), and finally for the *unstable* system we had $a_2 = 5.9$ au and $e_3 = 0.551$.

for this system is consistent with a dynamical origin. They suggested that a third outer companion is expected to reside far away and used the inner two planets' obliquities to constrain their inclinations. Follow-up radial velocity measurements estimated that a third companion indeed exists with a period of 1000 d and a minimum mass of 5.6 M_J (e.g. Otor et al. 2016). Here, we show that indeed a $\sim$5 M_J planet can exist at $\sim$3 au, with a range of possible eccentricities up to 0.9. A more massive planet can still exist at $\sim$3 au with a possible range of eccentricities up to slightly below $e_3 \sim 0.8$. This example of a tightly packed system yields the expected result, i.e. a large part of the parameter space is allowed to have an inclined companion, as depicted in Fig. 4 in the top right panel. In the presence of an inclined companion, the inner two planets will most likely have non-negligible obliquities, as was postulated by Li et al. (2014b).

(iii) *Kepler-88* is a star of, approximately, one solar mass. It has been observed to be orbited by two planets. The first planet is Earth-like ($m_1 \sim 0.85\ \mathrm{M}_\oplus$) and the second planet is comparable to Jupiter ($m_2 \sim 0.67\ \mathrm{M}_J$). Together, the two planets form a compact inner system with negligible eccentricities (e.g. Nesvorný et al. 2013; Barros et al. 2014; Delisle et al. 2017). In Fig. 4, left middle panel, we show that an inclined planet can exist in large parts of the parameter space. For example, a massive companion ($\sim$20 M_J) can exist beyond 2 au with an eccentric orbit ($\sim$0.7).

(iv) *Kepler-109* is a star that also has, approximately, one solar mass (1.07 $\mathrm{M}_\odot$) and two planets orbiting it in a compact

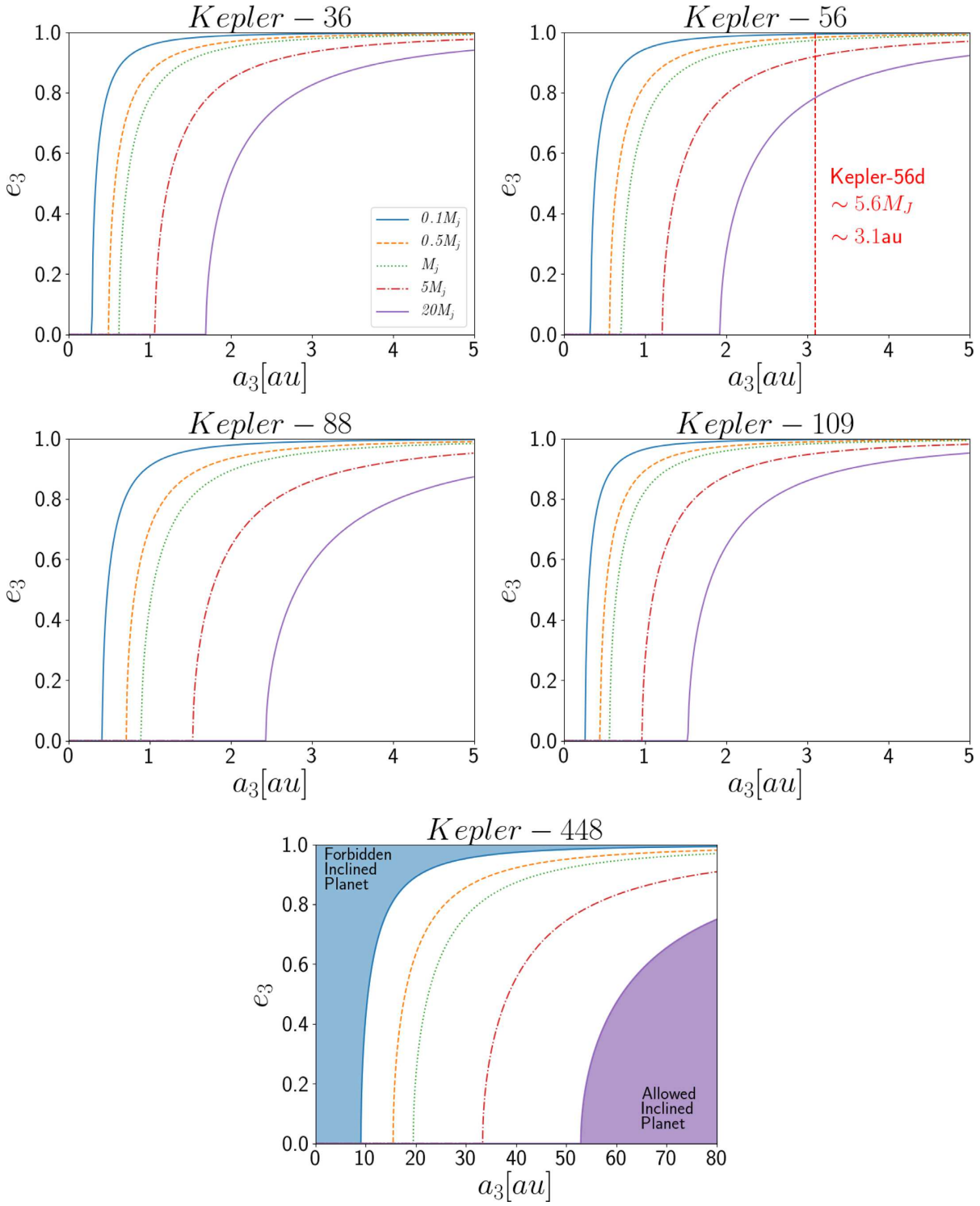

Figure 4. *The parameter space of hidden friends for a few observed systems*. Here, we consider the companion's eccentricity e_3 and separation a_3 for five Kepler systems. For each of the systems, we plot the stability criterion $e_{3,c}(f_{LL,min})$, for the different companion masses. *Note that this time we have varied a_3 rather than a_2 to predict parameter spaces in which known inner systems can exist*. Changing the dependent parameters for these cases yields a different shape of the stability curve when compared to Fig. 2. In particular, we consider companion mass of (from top to bottom), 0.1, 0.5,1, 5, and 20 M_J, with line styles indicated in the legend of the top left plot. The stable region exists below *each* curve and the instability region resides above each curve. (For Kepler-448, we shaded both the stable and unstable regions below the curve corresponding to a 20 M_J companion and above the curve corresponding to a 0.1 M_J companion, respectively.) For each system, we used the observed parameters in equation (12) to generate the contours. The observed parameters we used for the inner planets are specified in Table 1. We note that a third companion was reported to Kepler-56, with a minimum mass of 5.6 M_J, which yields a 3.1 au separation (Otor et al. 2016). This constrains the eccentricity of the companion to lie on a vertical line of a constant semimajor axis in the parameter space. As such, we overplotted Kepler-56d on the top right panel (dashed line).

Table 1. Observable parameters of the example systems. The observations are adopted from *Kepler-36*: Carter et al. (2012). *Kepler-56*: Huber et al. (2013) and Otor et al. (2016). *Kepler-88*: Nesvorný et al. (2013), Barros et al. (2014), and Delisle et al. (2017). *Kepler-109*: Marcy et al. (2014), Van Eylen & Albrecht (2015), and Silva Aguirre et al. (2015). *Kepler-419*: Dawson et al. (2012, 2014), and Huang, Wu & Triaud (2016). *Kepler-448*: Bourrier et al. (2015), Johnson et al. (2017), and Masuda (2017).

Name	SMA (au)	Mass (M_J)	Eccentricity
Kepler-36b	0.12	0.015	<0.04
Kepler-36c	0.13	0.027	<0.04
Kepler-56b	0.103	0.07	–
Kepler-56c	0.17	0.57	–
Kepler-88b	0.097	0.027	0.06
Kepler-88c	0.15	0.62	0.056
Kepler-109b	0.07	0.023	0.21
Kepler-109c	0.15	0.07	0.03
Kepler-419b	0.37	2.5	0.83
Kepler-419c	1.68	7.3	0.18
Kepler-448b	0.15	10	0.34
Kepler-448c	4.2	22	0.65

configuration, having a small mutual inclination (Marcy et al. 2014; Silva Aguirre et al. 2015; Van Eylen & Albrecht 2015). However, the eccentricity of the innermost planet is not as negligible as the secondary's ($e_1 \sim 0.21 > e_2 \sim 0.03$), but does not yield a violation of the approximation. We show the stability bounds within the (e_3, a_3) parameter space for this system in the middle right panel of Fig. 4. There it can be seen that this system can exist in the presence of an eccentric companion with 20 M_J, so long as the companion is beyond 3 au.

(v) *Kepler-419* is a 1.39 $M_\odot$ mass star which is orbited by two Jupiter-sized planets with non-negligible eccentricities and low mutual inclinations (e.g. Dawson et al. 2012, 2014; Huang et al. 2016). The large, observed eccentricities of the planets violate the assumption that the eccentricities are sufficiently small. Recall that this assumption was used to derive the stability criterion in equation (10). Furthermore, the quadrupole time-scale for precession induced by Kepler-419c on Kepler-419b is comparable to that of Laplace–Lagrange's. Thus, a distant massive companion is expected to excite the two planets' eccentricities and inclinations. When the mutual inclination between the two inner planets is large, the second planet can further excite the innermost planet's eccentricity, thus rendering the system unstable. We have verified, numerically, the instability of the system is consistent with the breakdown of our criterion. We did this for several systems with far away companions with masses varying from 1, 5, and 20 M_J. Thus, we suggest that a massive inclined companion can probably be ruled out for this system. Since our stability criterion is violated here, it is not necessary to show its parameter space in a plot. On the other hand, a smaller companion is not expected to cause secular excitations in the eccentricities of more massive planets, since the inner system will excite its eccentricity and inclination (e.g. inverse EKL Naoz et al. 2017; Zanardi et al. 2017; Vinson & Chiang 2018). Therefore, the existence of a smaller inclined companion cannot be ruled out.

(vi) *Kepler-448* is a 1.45 $M_\odot$ star orbited by a 10 M_J warm Jupiter (Bourrier et al. 2015; Johnson et al. 2017). Recently, there was a reported discovery of a massive companion (∼22 M_J) with a rather hierarchical configuration (Masuda 2017). The hierarchical nature of the inner system yields a more limited range of separations to hide a companion, see Fig. 4, in the bottom panel. On the other hand, the large masses of Kepler-448b and Kepler-448c imply that a small planetary inclined companion can still exist with negligible implications on the inner system. In fact, one would expect that the inner system will largely affect a less massive companion (e.g. Naoz et al. 2017; Zanardi et al. 2017, 2018; Vinson & Chiang 2018).
The relatively large observed eccentricity value of Kepler-448c can raise the question of the validity of the Laplace–Lagrange approximation of small eccentricities. After using the Gaussian averaging method for several extreme systems with fixed $m_3 = 20$ M_J, but different e_3, we found consistency with the stability curve. This was true even for the large eccentricity value of Kepler-448c. Moreover, for stable systems, the Laplace–Lagrange behaviour of small eccentricity oscillations still captures the dynamics of the system.

4 DISCUSSION

We have analysed the stability of four-body hierarchical systems, where the forth companion is set far away ($a_3 \gg a_2, a_1$). Specifically, we focus on three planet systems, for which the two inner planets reside in a relatively close configuration and have an inclined, far away, companion. Observations have shown that multiple tightly packed planetary configurations are abundant in our Galaxy. These systems may host a far away companion, which might be inclined or even eccentric. An inclined perturber can excite the eccentricity of planets in the inner system via the EKL mechanism, which can ultimately destabilize the system.

We have analytically determined a stability criterion for two-planet systems in the presence of an inclined companion (equation 10). This criterion depends on the initial conditions of the inner planetary system and on the outer orbit's mass, eccentricity, and separation. It is thus straightforward to generalize it to $n > 2$ inner planetary systems. We then numerically integrated a set of similar systems using the Gauss's averaging method, varying only the outer companion's eccentricity e_3 and the second planet's separation a_2. We have characterized each numerical integrated systems' stability and showed that stable systems are consistent with our analytical criterion.

A system will remain stable if the time-scale for angular momentum exchange between the two inner orbits takes place faster than eccentricity excitations that might be induced by a far away, inclined, companion. When the system is stable, the two inner orbits have minimal eccentricity modulations and their inclinations, with respect to their initial normal orbit, remained aligned to one another. An example of such a system is depicted in the left-hand panels of Fig. 3.

Assuming the normals of the inner orbits are initially parallel to the stellar axis allows precession of the nodes to be interpreted as obliquity variations. Thus, a non-negligible obliquity for two (or more) tightly packed inner orbits may be a signature of an inclined, distant, companion (e.g. Li et al. 2014b). The obliquity, in this case, oscillates during the system's dynamical evolution, which can have large implications on the habitability of the planets (e.g. Shan & Li 2017).

On the other hand, a system will destabilize if the precession induced by the outer companion is faster than the precessions caused by interactions between the inner bodies. In this case, the two inner planets will exhibit large eccentricity excitations accompanied with large inclination oscillations (see e.g. right-hand panels in Fig. 3). In this type of system, each planet undergoes nearly independent EKL oscillations, and thus extremely large eccentricity values can be expected, as well as chaos (e.g. Naoz et al. 2013a; Teyssandier et al. 2013; Li et al. 2014a).

We also showed (e.g. Fig. 2, green band) that the stability criterion includes a transition zone, where systems are likely to develop large eccentricity, leading to close orbits. Systems close to the transition zone, or in the transition zone, can be stable for long period of time, and develop instability very late in the evolution. We show an example for such a system in the middle column of Fig. 2. In this example, the system stayed stable for slightly more than a Gyr and developed an instability that leads to orbit crossing after ∼1.5 Gyr.

We note that our analysis did not include general relativistic or tidal effects between the planets and the star because, typically, including them will further stabilize systems. General relativistic precession tends to suppress eccentricity excitations if the precession takes place on a shorter time-scale than the induced gravitational perturbations from a companion (e.g. Naoz et al. 2013b). Also, tidal precession tends to suppress eccentricity excitations (Fabrycky & Tremaine 2007; Liu, Muñoz & Lai 2015). These suppression effects become more prominent the closer the inner orbits are to the host star. Thus, if eccentricity excitations from the companion take place on a longer time-scale than general relativity or tidal precession the system will remain stable.

Finally, as a proof-of-concept, we used our stability criterion to predict the parameter space in which a hidden inclined companion can reside for four Kepler systems (see Fig. 4). The systems we consider were Kepler-419, Kepler-56, Kepler-448, and Kepler-36. These systems represent a range of configurations, from tightly packed systems with small or super-Earth mass planets to potentially hierarchical systems with Jupiter mass planets. A notable example is Kepler-56, where the recently detected third planet was reported to have a minimum mass of 5.6 M_J, and a ∼1000 d orbit. Such a system indeed resides in the predicted stable regime. Furthermore, given a mass for the Kepler-56d, we can limit its possible eccentricity.

ACKNOWLEDGEMENTS

We thank the referee for useful comments. PD acknowledges the partial support of the Weyl Undergraduate Scholarship. SN acknowledges the partial support of the Sloan fellowship. BMH acknowledges the support of the Eugene V. Cota-Robles Fellowship and the Graduate Deans Scholar Award. Simulations in this paper made use of the REBOUND code which can be downloaded freely at http://github.com/hannorein/rebound.

REFERENCES

Antognini J. M. O., 2015, MNRAS, 452, 3610
Ballard S., Johnson J. A., 2016, ApJ, 816, 66
Barros S. C. C. et al., 2014, A&A, 561, L1
Batalha N. M. et al., 2013, ApJS, 204, 24
Batygin K., Laughlin G., 2008, ApJ, 683, 1207
Batygin K., Laughlin G., 2015, Proc. Natl. Acad. Sci., 112, 4214
Becker J. C., Adams F. C., 2016, MNRAS, 455, 2980
Becker J. C., Adams F. C., 2017, MNRAS, 468, 549
Borucki W. J. et al., 2011, ApJ, 736, 19
Bourrier V. et al., 2015, A&A, 579, A55
Bryan M. L. et al., 2016, ApJ, 821, 89
Burke C. J. et al., 2015, ApJ, 809, 8
Carter J. A. et al., 2012, Science, 337, 556
Christiansen J. L. et al., 2015, ApJ, 810, 95
Dawson R. I., Johnson J. A., Morton T. D., Crepp J. R., Fabrycky D. C., Murray-Clay R. A., Howard A. W., 2012, ApJ, 761, 163
Dawson R. I. et al., 2014, ApJ, 791, 89
Delisle J.-B., Correia A. C. M., Leleu A., Robutel P., 2017, A&A, 605, A37
Dressing C. D., Charbonneau D., 2013, ApJ, 767, 95
Fabrycky D., Tremaine S., 2007, ApJ, 669, 1298
Fang J., Margot J.-L., 2013, ApJ, 767, 115
Fienga A., Laskar J., Kuchynka P., Manche H., Gastineau M., Le Poncin-Lafitte C., 2009, in Heydari-Malayeri M., Reyl'E C., Samadi R., eds, SF2A-2009: Proceedings of the Annual Meeting of the French Society of Astronomy and Astrophysics, held in Besançon, 2009 June 29–July 4, p. 105
Hansen B. M. S., 2017, MNRAS, 467, 1531
Howard A. W. et al., 2010, Science, 330, 653
Howard A. W. et al., 2012, ApJS, 201, 15
Huang C., Wu Y., Triaud A. H. M. J., 2016, ApJ, 825, 98
Huang C. X., Petrovich C., Deibert E., 2017, AJ, 153, 210
Huber D. et al., 2013, Science, 342, 331
Inamdar N. K., Schlichting H. E., 2016, ApJ, 817, L13
Innanen K. A., Zheng J. Q., Mikkola S., Valtonen M. J., 1997, AJ, 113, 1915
Johansen A., Davies M. B., Church R. P., Holmelin V., 2012, ApJ, 758, 39
Johnson M. C., Cochran W. D., Addison B. C., Tinney C. G., Wright D. J., 2017, AJ, 154, 137
Jontof-Hutter D., Weaver B. P., Ford E. B., Lissauer J. J., Fabrycky D. C., 2017, AJ, 153, 227
Knutson H. A. et al., 2014, ApJ, 785, 126
Kozai Y., 1962, AJ, 67, 591
Li G., Naoz S., Holman M., Loeb A., 2014a, ApJ, 791, 86
Li G., Naoz S., Valsecchi F., Johnson J. A., Rasio F. A., 2014b, ApJ, 794, 131
Lidov M. L., 1962, Planet. Space Sci., 9, 719
Lissauer J. J. et al., 2011, ApJS, 197, 8
Lithwick Y., Wu Y., 2011, ApJ, 739, 31
Lithwick Y., Xie J., Wu Y., 2012, ApJ, 761, 122
Liu B., Muñoz D. J., Lai D., 2015, MNRAS, 447, 747
Marcy G. W. et al., 2014, ApJS, 210, 20
Masuda K., 2017, AJ, 154, 64
Mayor M. et al., 2011, preprint (arXiv:1109.2497)
Minton D., Malhotra R., 2011, in EPSC-DPS Joint Meeting 2011, held in Nantes, 2011 October 2–7, p. 591
Morbidelli A., 1994, Planet. Space Sci., 42, 301
Morton T. D., Bryson S. T., Coughlin J. L., Rowe J. F., Ravichandran G., Petigura E. A., Haas M. R., Batalha N. M., 2016, ApJ, 822, 86
Mullally F. et al., 2015, ApJS, 217, 31
Murray C. D., Dermott S. F., 2000, Solar System Dynamics. Cambridge Univ. Press, Cambridge
Mustill A. J., Davies M. B., Johansen A., 2017, MNRAS, 468, 3000
Naoz S., 2016, ARA&A, 54, 441
Naoz S., Farr W. M., Lithwick Y., Rasio F. A., Teyssandier J., 2011, Nature, 473, 187
Naoz S., Farr W. M., Lithwick Y., Rasio F. A., Teyssandier J., 2013a, MNRAS, 431, 2155
Naoz S., Kocsis B., Loeb A., Yunes N., 2013b, ApJ, 773, 187
Naoz S., Li G., Zanardi M., de Elía G. C., Di Sisto R. P., 2017, AJ, 154, 18
Neron de Surgy O., Laskar J., 1997, A&A, 318, 975
Nesvold E. R., Naoz S., Vican L., Farr W. M., 2016, ApJ, 826, 19
Nesvorný D., Kipping D., Terrell D., Hartman J., Bakos G. Á., Buchhave L. A., 2013, ApJ, 777, 3
Otor O. J. et al., 2016, AJ, 152, 165
Petigura E. A., Howard A. W., Marcy G. W., 2013, Proc. Natl. Acad. Sci., 110, 19273
Petrovich C., Tremaine S., Rafikov R., 2014, ApJ, 786, 101
Pu B., Lai D., 2018, MNRAS, 478, 197
Pu B., Wu Y., 2015, ApJ, 807, 44
Rein H., Liu S.-F., 2012, A&A, 537, A128
Saillenfest M., Fouchard M., Tommei G., Valsecchi G. B., 2017, Celest. Mech. Dyn. Astron., 129, 329

Scholl H., Froeschle C., 1986, A&A, 170, 138
Shan Y., Li G., 2017, LPI Contrib., 2042, 4075
Silva Aguirre V. et al., 2015, MNRAS, 452, 2127
Sridhar S., Touma J. R., 2016, MNRAS, 458, 4129
Teyssandier J., Naoz S., Lizarraga I., Rasio F. A., 2013, ApJ, 779, 166
Touma J. R., Tremaine S., Kazandjian M. V., 2009, MNRAS, 394, 1085
Van Eylen V., Albrecht S., 2015, ApJ, 808, 126
Vinson B. R., Chiang E., 2018, MNRAS, 474, 4855
Volk K., Gladman B., 2015, ApJ, 806, L26
Williams J. G., Faulkner J., 1981, Icarus, 46, 390
Youdin A. N., 2011, ApJ, 742, 38
Zanardi M., de Elía G. C., Di Sisto R. P., Naoz S., Li G., Guilera O. M., Brunini A., 2017, A&A, 605, A64
Zanardi M., de Elía G. C., Di Sisto R. P., Naoz S., 2018, A&A, 615, A21

This paper has been typeset from a TEX/LATEX file prepared by the author.